PLOS ONE

RESEARCH ARTICLE

Vertical distribution of methanotrophic archaea in an iron-rich groundwater discharge zone

Katsunori Yanagawa[1]*, Misaki Okabeppu[1], Sakiko Kikuchi[2], Fumito Shiraishi[3], Yumiko Nakajima[4], Akihiro Kano[5]

1 Faculty of Environmental Engineering, The University of Kitakyushu, Kitakyushu, Fukuoka, Japan, **2** Kochi Institute for Core Sample Research, Institute for Extra-cutting-edge Science and Technology Avant-garde Research (X-star), Japan Agency for Marine-Earth Science and Technology (JAMSTEC), Nankoku, Kochi, Japan, **3** Earth and Planetary Systems Science Program, Graduate School of Advanced Science and Engineering, Hiroshima University, Higashi-Hiroshima, Hiroshima, Japan, **4** Central Institute of Radioisotope Science and Safety Management, Kyushu University, Fukuoka, Japan, **5** Department of Earth and Planetary Science, Graduate School of Science, The University of Tokyo, Bunkyo-ku, Tokyo, Japan

* kyanagawa@kitakyu-u.ac.jp

Citation: Yanagawa K, Okabeppu M, Kikuchi S, Shiraishi F, Nakajima Y, Kano A (2025) Vertical distribution of methanotrophic archaea in an iron-rich groundwater discharge zone. PLoS ONE 20(2): e0319069. https://doi.org/10.1371/journal.pone.0319069

Editor: Mohamed Farghali, Kobe University: Kobe Daigaku, JAPAN

Received: October 23, 2024

Accepted: January 27, 2025

Published: February 24, 2025

Data availability statement: All relevant data are within the manuscript and its Supporting Information files.

Funding: KY. Grant Numbers 17K18808, 20K05404, and 24K07204. Japan Society for the Promotion of Science (JSPS) KAKENHI. The funders had no role in study design, data collection and analysis, decision to publish, or preparation of the manuscript.

Abstract

Anaerobic oxidation of methane coupled to iron reduction (Fe-AOM) is a crucial process for methane removal in terrestrial environments. However, the occurrence of Fe-AOM in natural environments is rare, and the mechanisms behind the direct coupling of methane oxidation and iron reduction remain poorly understood. In this study, we investigated the environmental factors influencing the distribution of methanotrophic archaea in an iron-rich zone of a freshwater pond in Hiroshima Prefecture, Japan. High concentration of dissolved ferrous iron supplied by groundwater discharge led to considerable ferrihydrite precipitation. Pore water methane increased with sediment depth, while nitrate and sulfate concentrations were near detection limits throughout the sediment column. The coexistence of ferric iron and methane suggests the ongoing process of Fe-AOM. Tracer-based experiments using ^{14}C showed potential Fe-AOM rates up to 110 pmol mL^{-1} day^{-1}. Throughout the sediment core, except at the surface, PCR-based molecular ecological analyses of the 16S rRNA gene and functional genes for anaerobic oxidation of methane revealed abundant sequences belonging to the family "*Candidatus* Methanoperedenaceae". These geochemical and microbiological findings suggest that Fe-AOM plays a key role in biogeochemical cycles of iron and methane, positioning this environment as a modern analogue of early Earth conditions.

Introduction

Methane (CH_4) is a major greenhouse gas, and its global warming potential is approximately 30 times greater than that of carbon dioxide (CO_2) [1]. Global methane emissions from natural sources are estimated to be 218 Tg per year [2], with atmospheric methane concentrations increasing by 5.7 to 17.9 ppb annually over the past decade [3]. Methane is produced from various natural sources, including marine and freshwater sediments, wetlands, inland aquatic

Competing interests: The authors have declared that no competing interests exist.

ecosystems, rice paddy soils, organic-rich landfills, and animal digestive systems. Among these emission sites, freshwater systems are considered as a major source of methane emissions to the atmosphere, contributing approximately 53% of the total global emissions [4].

Methane fluxes from natural environments are largely mitigated under anoxic conditions by a microbial process called anaerobic oxidation of methane (AOM), which operates via a reverse methanogenesis pathway. In marine sediments, AOM is typically coupled with sulfate (SO_4^{2-}) reduction [5,6]. Sulfate-AOM serves as the main sink for methane in marine environments, removing 70–90% of the methane released into the overlying seawater and atmosphere [7,8]. However, sulfate concentrations are considerably low in freshwater systems such as lakes and rivers [9], making sulfate-dependent processes less crucial in these systems [10,11]. Thermodynamic considerations based on free energy yield suggest that more favorable electron acceptors, such as nitrite (NO_2^-), nitrate (NO_3^-) [12], Mn(IV) [13], iron oxides [14–17], As(V) [18], and humic substances [19,20] could oxidize methane under anaerobic conditions. Among these, AOM coupled with metal oxides, such as Fe(III) reduction (Fe-AOM), has been identified as a key process for methane regulation in terrestrial [11], coastal [21,22], and marine environments [23].

Anaerobic methanotrophic archaea belonging to ANME-1, -2, and -3 are responsible for sulfate-AOM in various marine environments [5]. By contrast, Fe-AOM in freshwater environments is primarily mediated by members of the family "*Candidatus* Methanoperedenaceae" [15,24–26]. This group of archaea belongs to the ANME-2d cluster, previously described as AOM-associated archaea (AAA) [10], and consists solely of uncultured representatives from terrestrial habitats, although some marine sequences have also been identified [27]. Unlike in previous studies reporting that ANME show syntrophic associations with bacterial partners, *Ca.* Methanoperedenaceae can perform Fe-AOM without bacterial partners [15] and can utilize various electron acceptors other than Fe(III), such as NO_3^- [12], SO_4^{2-} [26,28], Mn(IV) [13], Cr(VI) [29], and humic substances [19].

Although many studies have been conducted on Fe-AOM, most of them have focused on enrichment cultures for archaeal methanotrophs. Thus, the role of *Ca.* Methanoperedenaceae in natural methane mitigation remains unclear. Consequently, the key factors controlling Fe-AOM and the environmental distribution of these methanotrophs also remain relatively unexplored. The occurrence of Fe-AOM in natural environments needs to be further explored to determine which forms of iron oxide act as electron acceptors for Fe-AOM [30]. In this study, we investigated freshwater sediments from a groundwater discharge zone in Budo Pond, Hiroshima Prefecture, Japan. Owing to the supply of Fe^{2+}-rich underground fluids, ferruginous sediments primarily composed of biogenic ferrihydrite are established at the mouth of the groundwater discharge in Budo Pond [31–33]. These deposits were observed throughout the year within an area several meters from the discharge point. Deep sediments are characterized by anaerobic conditions with abundant methane produced by methanogenic archaea [31]. Therefore, the study site provides an ideal habitat for microorganisms involved in Fe-AOM. In the present study, based on a detailed vertical analysis conducted at centimeter-scale intervals in iron-rich habitats using an integrated approach, including geochemistry, stable isotope analysis, radiotracer experiments, microbial abundance quantification, and molecular ecology, we examined the distribution and favorable niches of *Ca.* Methanoperedenaceae, the key microbes controlling methane reduction via Fe-AOM.

Materials and methods

Sample collection and processing

Budo Pond is located on the campus of Hiroshima University, Japan (34°24.060 N, 132°42.790 E) (S1 Fig). Sample collection was conducted with the approval of Hiroshima University.

Before sampling the sediment core, the pH, temperature, dissolved oxygen (DO), and redox potential (Eh) of the surface water were measured on-site using a portable sensor (D-75, Horiba, Kyoto, Japan) equipped with individual electrodes. In August 2016, a sediment core was collected at 20 cm from the groundwater discharge point using an acrylic tube with an inner diameter of 6 cm. The core was immediately sectioned into 1–4 cm-thick slices for geochemical and molecular biological analyses using sterile spatulas. Samples for DNA analysis were stored at −80 °C in 1.5 mL microcentrifuge tubes. A portion of the sediment was placed in 50 mL conical tube and centrifuged to extract pore water. The supernatant was filtered through a 0.45 μm pore-size cellulose acetate filter and stored until further analysis. Another 1 mL portion of the sediment was placed in a 15 mL conical tube, fixed overnight at 4 °C with a 3.7% formaldehyde solution, and stored at −80 °C until microscopic examination. For AOM activity measurement, 5 mL of sediment samples were stored anaerobically at 4 °C in 30 mL glass vials, with the headspace replaced by argon gas.

Water geochemistry

The major cations (Na^+, Mg^{2+}, K^+, and Ca^{2+}) and anions (Cl^-, NO_3^-, and SO_4^{2-}) in the pore water were measured using ion chromatography (IC; Jasco Gulliver system, Jasco International Co., Ltd, Tokyo, Japan). The concentration of Mn^{2+} was evaluated using atomic absorption spectroscopy (AA-6200; Shimadzu, Kyoto, Japan). The concentrations of dissolved Fe^{2+} and hydrogen sulfide were measured spectrophotometrically using the ferrozine [34] and methylene blue [35] methods, respectively. Dissolved inorganic carbon (DIC) and methane were measured using the headspace gas method, as described previously [36], using a gas chromatograph (GC; Agilent 7820A) equipped with a thermal conductivity detector. The stable carbon isotopic compositions of DIC ($\delta^{13}C_{DIC}$) were measured using a conventional isotopic ratio mass spectrometer (IRMS; Thermo Finnigan Delta Plus XP) connected to a Flash EA 1112 Automatic Elemental Analyzer via a ConFlo III interface as described previously [37]. Total organic carbon (TOC) concentrations were determined using an elemental analyzer (CHN CORDER MT-6, Yanako). The $\delta^{13}C_{TOC}$ values were measured using an isotope ratio mass spectrometer (Isoprime VisION, Elementar) coupled with an elemental analyzer (vario PYRO cube, Elementar).

AOM rates

The potential of AOM was assessed using radioisotope tracer incubation experiments, as described previously [38,39]. In brief, 5 cm^3 of sediment samples were incubated at 20 °C for five days in darkness under a headspace gas filled with 200 kPa of methane and 1 MBq of ^{14}C-labeled methane (American Radiolabeled Chemicals, Inc., St. Louis, MO, USA). Two autoclaved samples were used as negative controls. To terminate the microbial activity and facilitate the release of CO_2 into the headspace, the samples were acidified with 1 mL of 6 N HCl. The radioactivity of a portion of reaction products (i.e., $^{14}CO_2$) in the headspace was determined using a gas chromatograph (Shimadzu GC8A, Shimadzu, Kyoto, Japan) equipped with a high-sensitivity radioactivity detector (RAGA Star, Raytest, Straubenhart, Germany). Potential AOM activities were calculated using following equations:

$$AOM\ rate = k \times C,$$

$$Turnover\ rate(k) = F \times \frac{a^{-14}CO_2}{a^{-14}CH_4} \times \frac{1}{t},$$

where C is the *in situ* methane concentration, F is the isotope fraction factor for AOM (1.06 [40]), a-$^{14}CO_2$ is the radioactivity of the produced $^{14}CO_2$, a-$^{14}CH_4$ is the radioactivity of the injected $^{14}CH_4$, and t is the incubation time (5 days). In this equation, the AOM rate is expressed as pmol CH_4 oxidized per mL sediment per day.

Prokaryotic 16S rRNA gene phylotype composition analysis

Microbial DNA was extracted directly from 0.2 g of sediment using the DNeasy PowerSoil Kit (Qiagen, Hilden, Germany). Microbial cells were mechanically crushed for 10 min using a μT-01 bead crusher (TAITEC, Koshigaya, Japan) as described previously [41]. The extracted DNA samples were stored at −80 °C for further analyses. Universal primers 515F and 806R [42] were used to amplify the hypervariable V4 region of the prokaryotic 16S rRNA gene. Amplification was performed using MightyAmp DNA Polymerase Ver.3 (Takara Bio) and Biometra TAdvanced 96 SG (Biometra, Göttingen, Germany). The thermal cycling conditions comprised an initial denaturation step at 98 °C for 2 min, followed by 40 cycles of denaturation at 98 °C for 30 s, annealing at 55 °C for 30 s, extension at 68 °C for 30 s, and a final extension at 68 °C for 5 min. An equimolar mixture of all PCR products was sent to FASMAC Co., Ltd. for 2 × 300 bp paired-end sequencing on the Illumina MiSeq platform using the Illumina MiSeq Reagent Kit v3. Downstream analysis of sequence reads was performed using QIIME 2 2020.8 [43], including DADA2 [44]. The 16S rRNA gene amplicon sequences were aligned with MAFFT [45] and used to construct a phylogenetic tree using FastTree [46]. Taxonomic identification of the representative sequences was performed using the SILVA 138 database (silva-138-99-nb-classifier). Alpha and beta diversity analyses were performed using core-metrics-phylogenetic plugin in QIIME 2. Beta diversity distances were determined based on Bray-Curtis distances. Raw sequence reads were deposited in the Sequence Read Archive (SRA) under the accession number DRA016493.

Microbial cell and gene abundance

Approximately 0.2 g of the sediment sample was preserved in a 3% formaldehyde solution for 2 h at room temperature. The fixed microbial cells were filtered onto 0.2 μm-pore-size polycarbonate membranes (Isopore Membrane, Merck Millipore, USA). To preserve the integrity of cell aggregates, no dispersing treatments, such as sonication, were applied prior to filtration. The cells were stained with 250 × SYBR Green I, and counted in triplicate, as described previously [47]. Microscopic images were captured at magnifications ranging from 400 × to 1000 × using an Eclipse 80i fluorescence microscope (Nikon, Tokyo, Japan) equipped with B-2A longpass filter cubes.

Quantification of total prokaryotic and archaeal 16S rRNA gene abundance was performed via quantitative PCR (qPCR) using universal and archaeal primer-probe sets [48] and an innuMIX qPCR MasterMix Probe and a real-time PCR system qTOWER^3 G touch (Analytik Jena AG, Germany). The thermal cycling conditions were as follows: 50 cycles of denaturation at 98 °C for 10 s, annealing at 50 °C (for the universal 16S rRNA gene) or 52 °C (for the archaeal 16S rRNA gene) for 45 s and an extension at 72 °C for 30 s. *mcrA* gene abundance was also determined using a specific primer set [49] and MightyAmp for Real-Time PCR (TaKaRa Bio, Inc., Otsu, Japan). The amplification conditions comprised 40 cycles of denaturation for 40 s at 94 °C, annealing at 52 °C for 30 s, and extension at 68 °C for 60 s. All qPCR assays were performed in triplicate. Details of the qPCR experiments are provided in S1 Table.

Clone library construction of *mcrA* genes

The *mcrA* gene fragments were amplified via PCR using MightyAmp DNA Polymerase Ver.3 (TaKaRa Bio, Inc., Otsu, Japan) and the specific primer set used for the qPCR analysis [49].

The amplified PCR products were purified, cloned, and sequenced as described previously [9]. The taxonomic affiliations of the *mcrA* gene sequences were determined based on neighboring reference sequences in phylogenetic tree, which was constructed using a custom-curated *mcrA* dataset with the ARB software package [50]. The *mcrA* gene sequences reported in this study have been deposited in the DDBJ/EMBL/GenBank databases under accession numbers LC770274–LC770306.

Results and discussion

Geochemical features of Budo Pond sediment

The temperature of the discharged groundwater was 17.3 °C, slightly higher than the average annual temperature of 16 °C [31]. The pH was slightly acidic at 6.3, with dissolved oxygen concentration of 0.75 mg/L (23.4 μM) and an Eh value of −23 mV. CH_4 concentrations were significantly lower in the shallow sediments but higher in the deeper sediments, reaching up to 850 μM at a depth of 18.5 cm (Fig 1 and S2 Table). Dissolved iron concentration (Fe^{2+}) was 740 μM at 1.5–3.5 cm depths but decreased to 70 μM at 18.5 cm from the surface. The positive iron peak corresponded to the negative methane peak. The concentrations of SO_4^{2-}, NO_3^-, and Mn were less than 48.5, 11.4, and 34.9 μM, respectively. No considerable changes in the vertical profiles of SO_4^{2-}, NO_3^-, and Mn concentrations were observed in relation to the CH_4 profile. Furthermore, sulfide concentration was below the detection limit of 0.5 μM at all depths. The depth profile of dissolved inorganic carbon (DIC), one of the major end-products of AOM, mirrored the Fe^{2+} profile, increasing from 1.8 mM (0 cm depth) to 2.8 mM (2.5 cm) before decreasing to approximately 1 mM at 15.5 cm. Calcium (Ca^{2+}) concentrations exceeded 0.2 mM in the upper sediment but were reduced by half in the deepest part (S2 Fig), consistent with the notion that Ca^{2+} are used to form calcium carbonates under high pH condition. In marine environments, high bicarbonate concentrations lead to the precipitation of calcium carbonate [8], which is often interpreted as a fossil signature of AOM [51,52]. The vertical distributions of other ions such as Na^+, K^+, and Cl^- showed no notable variation. These physicochemical characteristics suggest that iron reduction may play a key role in shaping the CH_4 profile. They are not only consistent with those previously reported at this discharge point [31–33] but also similar to findings from other iron-rich freshwater sediments where AOM occurs [28].

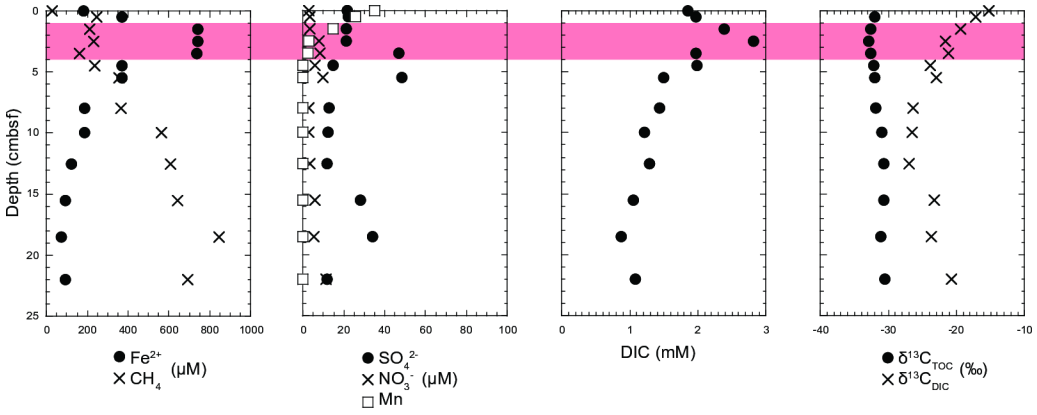

Fig 1. Depth profiles of pore water geochemistry in the Budo Pond sediment. The red-shaded layers indicate the depth range of high iron concentration.

https://doi.org/10.1371/journal.pone.0319069.g001

The stable carbon isotope compositions of the TOC and DIC were also determined. The $\delta^{13}C_{DIC}$ value of the surface pore water was −15.2‰ VPDB (Vienna Pee Dee Belemnite), likely affected by inorganic carbon in the pond water and the atmosphere. It significantly decreased to −23.9‰ VPDB at 4.5 cm depth (Fig 1). This steep decline could be attributed to the involvement of DIC derived from the oxidation of methane and/or organic materials in the sediment. According to a previous study [31], $\delta^{13}C_{methane}$ was −68.8‰ VPDB. TOC concentrations in the sediments were relatively high (0.4–4 wt%) (S2 Fig). The $\delta^{13}C_{TOC}$ values ranged from −32.9‰ to −30.5‰ VPDB (Fig 1), which are slightly lower than the values typically observed in freshwater sediments. The lowest value was observed at a depth of 2.5 cm, which was attributed to the influence of methanotroph-derived organic matter, as this depth corresponds to the potential Fe-AOM zone.

AOM activity

We explored the potential role of Fe(III) as a terminal electron acceptor in AOM using the sediment from Budo Pond. Experiments utilizing radiolabeled tracers revealed the maximum AOM rate of 110 pmol mL^{-1} day^{-1} (Fig 2). Given the high amounts of ferrihydrite in the sediments, Fe(III) was likely the primary electron acceptor and played a crucial role in methane removal. The AOM rates in this study were measured at 20°C, which is slightly higher than the in situ water temperature of 17.3°C. While this may have led to overestimation of the AOM rate, the values remain comparable to those reported in iron-amended incubation experiments conducted in terrestrial subsurface environments [53]. Although these rates were significantly lower than those reported for enrichment culture samples obtained from surface environments [15], this discrepancy is likely due to the differences in sample types (enrichment culture vs. natural environment) as well as the abundance and activity of anaerobic methanotrophs. The biological methane production rate in deeper sediments has not been investigated; however, the turnover rate observed in tracer experiments suggests that methane

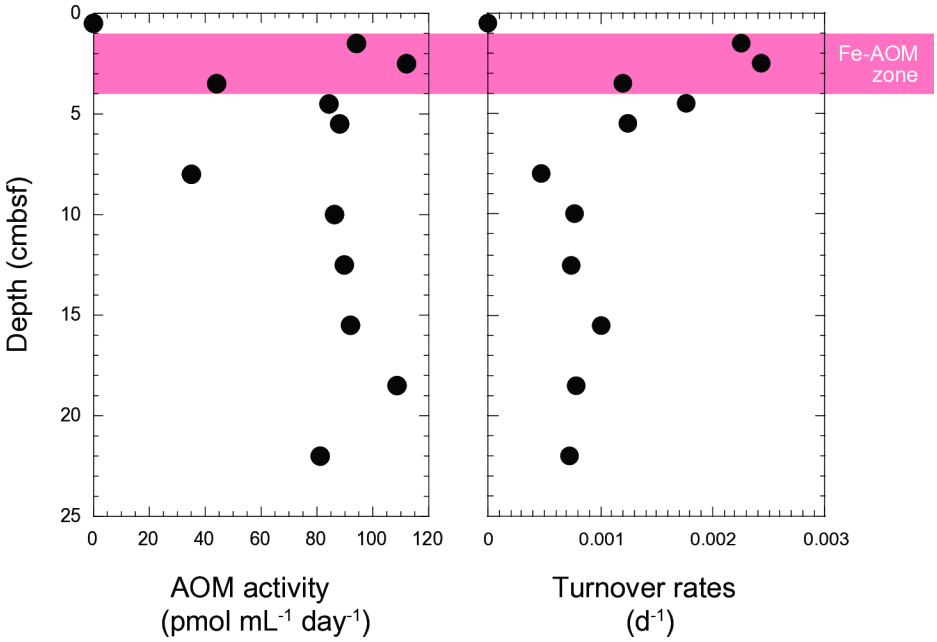

Fig 2. Depth profiles of potential AOM activity and turnover rates.

https://doi.org/10.1371/journal.pone.0319069.g002

in the studied core could be depleted through AOM within a few years (Fig 2). This finding underscores the importance of this process in regulating methane concentrations within freshwater systems.

16S rRNA gene-based microbial community structure

To identify the methanotrophic archaea potentially responsible for Fe-AOM at our study site, we analyzed the microbial community compositions of 12 sediment layers through amplicon sequencing targeting the V4 hypervariable region of the 16S rRNA gene fragments. A total of 877,716 quality-filtered sequences were obtained and used for further analysis (Fig 3 and S3 Table).

Members of genus *Ca.* Methanoperedens, within the class Methanosarcinia of the phylum Halobacterota, were detected in the 16S rRNA gene phylotype. They represent one of the most abundant archaeal populations at the genus level, comprising up to 4.7% of the total community composition. At the top surface, where oxic and low methane conditions prevailed, they accounted for only 0.2% of the community. No sequences of other archaeal methanotrophs were detected at any depth in the sediment core from Budo Pond. In contrast, methanogenic archaea constituted less than 0.4% of the microbial community throughout the sediment.

The vertical profile of the relative abundance of the 16S rRNA gene phylotype composition revealed that members belonging to the family Gallionellaceae predominated in the surface sediment, comprising up to 29.6% of all phylotypes. Most were classified within the genera Gallionella and Sideroxydans, indicating the dominance of Fe(II)-oxidizing bacteria, which is similar to the surface environment of many iron-rich freshwater systems [54]. Additionally, members of the genus Thiothrix in the family Thiotrichaceae accounted for 18.6% of the total community composition in the surface sediment. They are known for sulfur oxidization [55] despite the absence of sulfide in the pore water throughout the core.

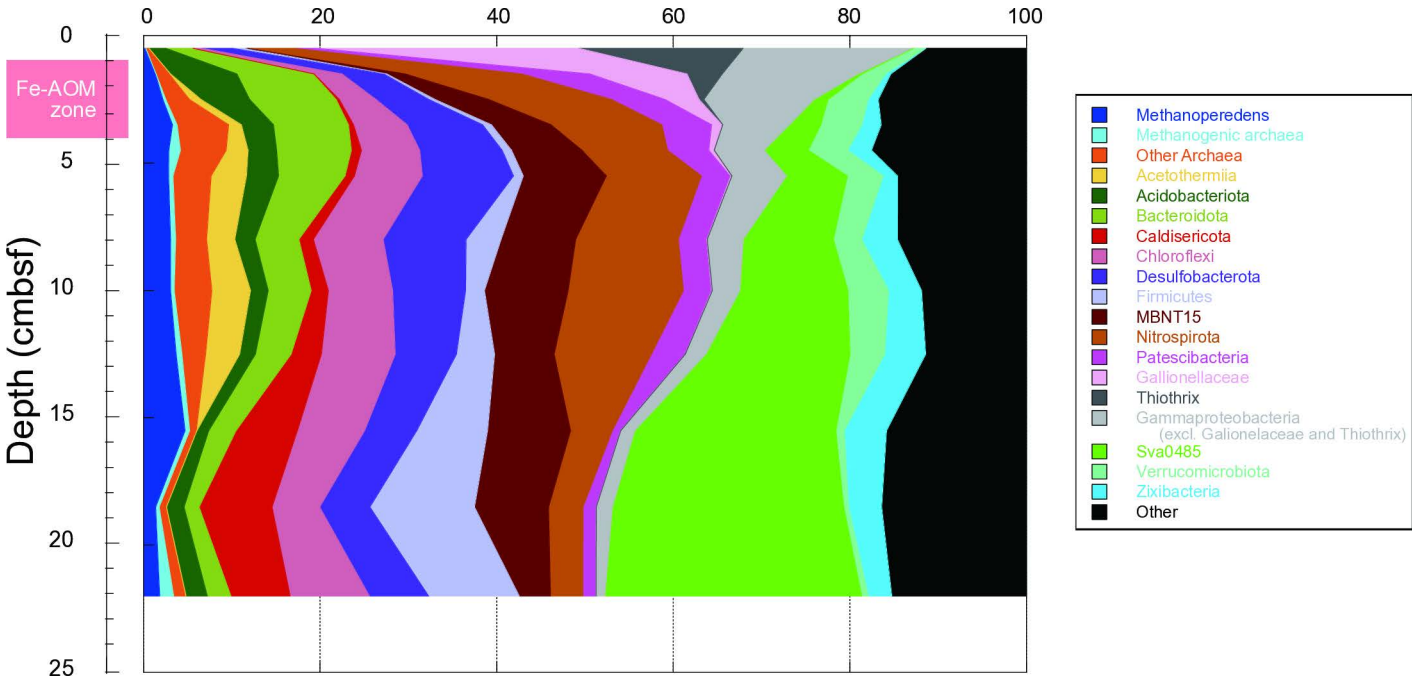

Fig 3. Taxonomic compositions of 16S rRNA gene sequences in the sediments. The width of the bars along the vertical axis corresponds to the actual range of each core section.

https://doi.org/10.1371/journal.pone.0319069.g003

In the middle core layers, the major phylotypes changed to the phyla Bacteroidetes, Chloroflexi, Desulfobacterota, Nitrospirota, MBNT15, Nitrospirota, Verrucomicrobiota, and Zixibacteria. Among the Desulfobacterota, members of the genus Syntrophus, known for their syntrophic lifestyle [56], were prominent and accounted for 3.4–4.5% at depths of 3.5–12.5 cm. The candidate phylum MBNT15 was abundant at depths of 2.5–18.5 cm. Most members perform dissimilatory iron reduction according to metagenomic analyses [57]. Members of the Verrucomicrobiota included the genus "*Candidatus* Omnitrophus," which accounted for 3.4–4% at depths of 10–12.5 cm. A previous report suggested that genetic potential of Omnitrophus is associated with magnetosome biosynthesis, sulfur oxidation, and carbon fixation [58]. Members of the phylum Zixibacteria were abundant in the deepest layers. They are considered potential participants in iron cycling within the continental subsurface [59]. Notably, previous research has specifically highlighted the iron-reducing metabolic capabilities of Zixibacteria in coastal sediments [60].

At the bottom of the core, community members shifted and the bacterial phyla Caldisericota, Firmicutes, and Sva0485 became more prominent. Members of Caldisericota were particularly dominant at a depth of 18.5 cm, comprising 8.3% of the overall community. These organisms are heterotrophs [61] and thrive on oxidized sulfur intermediates. Although these sulfur compounds could be provided by sulfur-oxidizing bacteria or by the oxidation of sulfides by ferric iron (Fe^{3+}) within the sediments, the concentrations of sulfides in the pore water were below the detection limits, suggesting a small-scale sulfur cycle. Below a depth of 18.5 cm, members of the phylum Firmicutes comprised more than 10.3% of the community. Notably, the uncultured Class D8A-2 accounted for more than 92% of Firmicutes, representing the majority. They possess the potential for syntrophic propionate oxidation [62]. The most notable increase in depth was observed in members of Sva0485, which accounted for 29.1% of the community at the deepest point of 22 cm. These have been described as most likely sulfate reducers or sulfur oxidizers, depending on the redox conditions [63]. Additionally, several genes related to the iron cycle have also been identified from the Sva0485 MAGs. Potential Fe(III)-reducing bacterial lineages commonly found in natural environments, such as Geobacteraceae [64], were detected as minor populations, each constituting less than 0.1% of the community.

The alpha diversity metrics including the number of observed features, the Shannon index, Pielou's evenness, and Faith's PD are shown in S3 Table and S3 Fig. These alpha diversity indices varied significantly with depth, showing a notable decreasing trend with greater depths. The beta diversity analysis suggested that the microbial community composition changed continuously with depth. (S4 Fig).

Quantitative analysis of microbial populations

Fluorescence microscopy revealed microbial cell concentrations ranging from 6.7×10^7 to 2.5×10^8 cells per mL of the sediment (Fig 4). All the observed cells appeared as individual entities (S5 Fig), indicating the absence of the ANME consortia with specific bacterial partners. The qPCR analysis showed similar levels of total prokaryotic 16S rRNA genes, ranging from 3.3×10^7 to 1.2×10^9 genes per gram of sediment. This supports the idea that most of cells observed under the microscope are prokaryotes. Archaeal 16S rRNA gene profiles followed a similar trend but were one to two orders of magnitude lower than those of prokaryotes, with values ranging from 2.6×10^6 to 2.1×10^8 genes per gram of sediment.

The abundance of *mcrA* gene, which is a key functional gene for AOM or methanogenesis, followed a similar pattern but was relatively lower than that of the archaeal 16S rRNA genes (Fig 4). The highest *mcrA* concentration was detected in shallow sediment (3.5 cm) with 4.5×10^7 copies per gram of sediment. The relative composition of the *mcrA* phylotypes

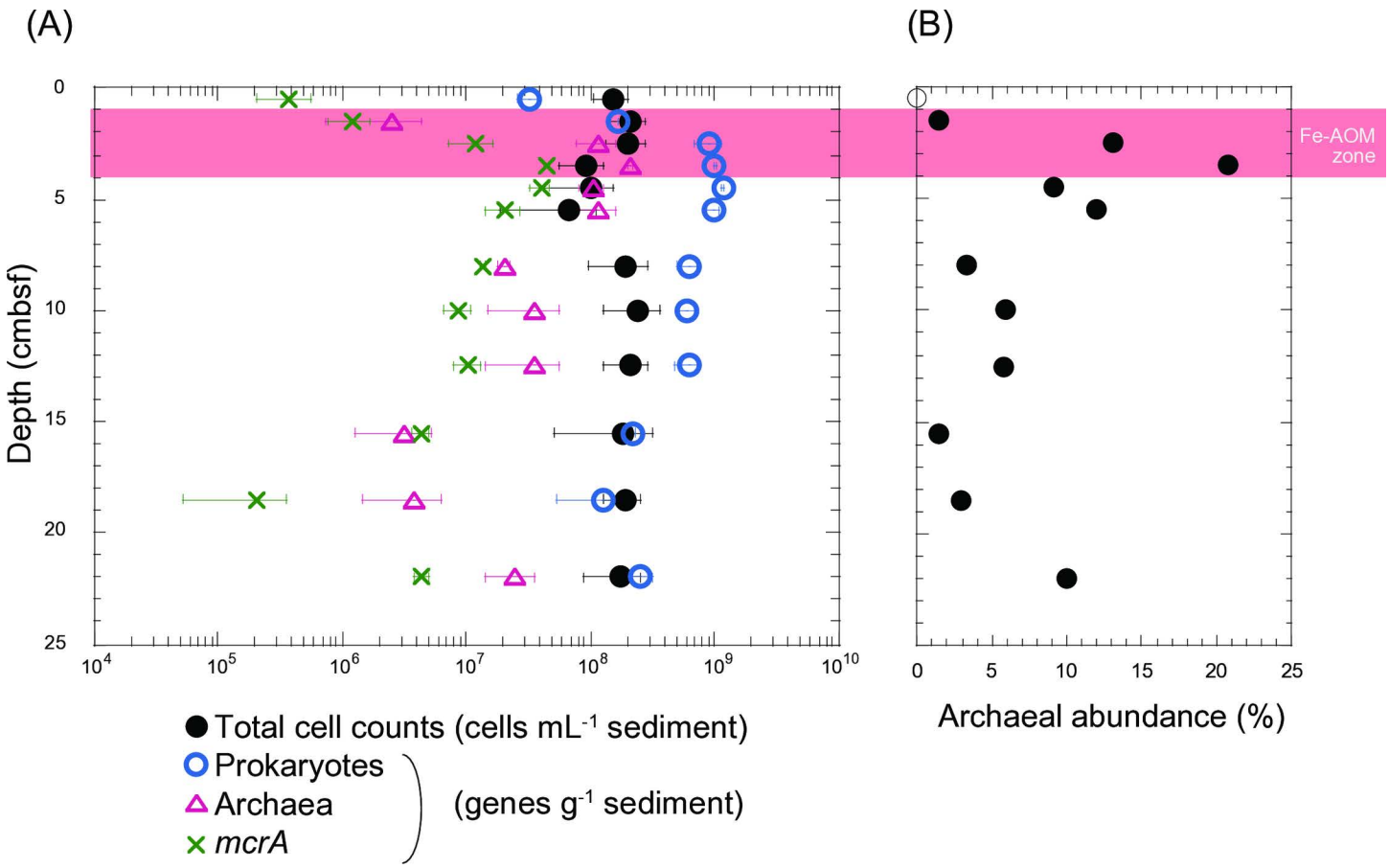

Fig 4. Microbial biomass in the Budo Pond sediment. (A) Total cell counts (black circles) and the 16S rRNA gene numbers of prokaryotes (blue circles), archaea (red triangles), and *mcrA* (green crosses) quantified by qPCR. (B) The relative archaeal abundances determined by the ratio of the number of archaeal 16S rRNA genes to that of total prokaryotic 16S rRNA genes. Open circles on the y-axes denote analyses below the detection limit.

https://doi.org/10.1371/journal.pone.0319069.g004

was determined through sequencing of the *mcrA* genes amplified (Fig 5). Phylogenetically, *mcrA* was categorized into several groups, including Methanoperedenaceae, Methanomicrobiales, Methanomassiliicoccus, Methanosaeta, and Verstraetearchaeota. At depths of approximately 1.5 to 3.5 cm, over 93% of the *mcrA* gene amplicons were associated with the Methanoperedenaceae.

Factors controlling Fe-AOM

The significant increase in pore water Fe^{2+} concentrations between 1.5 and 3.5 cm depths suggests that Fe(III) reduction occurred in the specific anoxic layer. This coincided with the positive peaks of DIC and Methanoperedenaceae *mcrA* gene abundance as well as negative methane trends, indicating that methane removal was coupled with dissimilatory iron reduction and simultaneous CO_2 generation. Additionally, the $\delta^{13}C_{TOC}$ value exhibited a slight peak and dropped down to −32.9 ‰ VPDB at 2.5 cm. These relatively low values measured in the AOM zone imply the active accumulation of methane-derived carbon in organic materials. The correlation between the gene abundance of Methanoperedenaceae *mcrA* and AOM rate further supports the role of Methanoperedenaceae in methane oxidation. This idea is corroborated by the fact that Methanoperedens is dominant in environments where Fe- AOM occurs

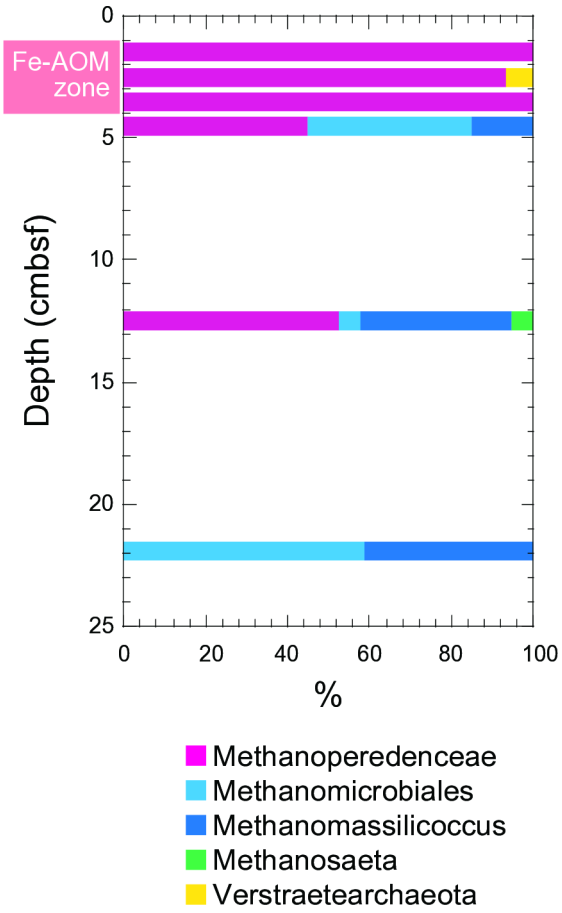

Fig 5. Phylogenetic affiliation of *mcrA* genes.

https://doi.org/10.1371/journal.pone.0319069.g005

[15,24,53]. Although the possibility of the involvement of NO_3^-, SO_4^{2-}, and Mn(IV) reduction cannot be entirely excluded, their concentrations did not provide a significant portion of the AOM in Budo Pond. These values were much lower than the Fe^{2+} concentrations. NO_3^- and SO_4^{2-}concentrations showed slight fluctuations, with no correlation to methane. Therefore, Fe(III) appears to be a thermodynamically favorable electron acceptor for AOM in Fe(III)-rich sediments. The exact mechanism of Fe(III) utilization by Methanoperedenaceae is not yet fully understood. In this study, no cell aggregates were observed using fluorescence microscopy, suggesting that there was no physical interaction between the Methanoperedenaceae archaeons and bacterial partners (S5 Fig). Some members of Methanoperedenaceae perform Fe-AOM via direct electron transfer without bacterial partners involving multi-heme c-type cytochromes [15,24]. This process is facilitated by an extracellular electron transport mechanism wherein electrons generated during methane oxidation are relayed through multi-heme c-type cytochromes to the terminal electron acceptors, such as ferrihydrite. Furthermore, it has been suggested that electrons might pass on to dissimilatory metal-reducing bacteria, such as *Shewanella oneidensis* [65].

Despite the low activity of our samples, the radiotracer-based incubation experiments revealed relatively high AOM rates at a depth of 2.5 cm. This aligned with the qPCR results, which showed a high abundance of Methanoperedenaceae *mcrA* at this depth. The availability of electron acceptors suggests that Fe(III) is a key factor controlling Fe-AOM activity in

surface sediments. Fe(III)-containing minerals might have formed from biotic or abiotic Fe^{2+} oxidation near the sediment surface. The 16S rRNA gene amplicon analysis suggested that members of Gallionellaceae contributed to Fe(II) oxidation in surface sediments, as shown in a previous study at this site [32]. The biogenic Fe(III) materials produced, known as stalks and sheaths, are composed of structurally less ordered and complex ferrihydrites and are characterized by large surface areas [66]. These less crystalline ferrihydrites are more susceptible to reduction by dissimilatory Fe(III)-reducing bacteria [67]. These biologically derived ferrihydrite-like materials were also abundant at the bottom of the core. In the deeper layers, Fe(III) is dissimilatorily reduced to Fe(II) through microbial processes, leading to the formation of secondary iron minerals, such as goethite and siderite [68–70]. In Budo Pond, both ferrihydrite and goethite coexist in deep sediments; however, the surface of ferrihydrite in deeper sediments is partially covered with goethite [31]. These findings suggest that while surface sediments provide specific physical and chemical conditions suitable for Fe-AOM, unfavorable conditions exist in deeper sediments. Indeed, the vertical profile of the *mcrA* gene and the Fe^{2+} concentration in pore water indicated that Fe-AOM is not occurring throughout the core but is limited to surface sediments at depths of 1.5–3.5 cm (Figs 1 and 4). We hypothesized that the encrustation of ferrihydrite surfaces by goethite is a likely reason why Methanoperedenaceae cannot access ferrihydrite, thereby reducing the potential activity of Fe-AOM.

Environmental significance of Fe-AOM in iron-rich sediments

Several previous studies have recognized Fe-AOM as an important methane removal process in various iron-rich environments based on geochemical evidence [16,21,22,71–74]. However, the microorganisms responsible for the metal-dependent AOM remain largely unknown. This study demonstrated that in freshwater sediments where methane and iron oxides coexist and potential electron acceptors, such as SO_4^{2-}, are almost absent, Fe-AOM serves as a significant methane sink, with Methanoperedenaceae identified as the primary microorganisms involved in this process. This allowed for a discussion on the importance of specific forms of iron and the quantitative distribution of the microorganisms involved. Consistent with our findings, Methanoperedenaceae have been reported as prominent candidates for Fe-AOM processes in low-sulfate, iron-rich environments such as the anoxic water column of Kabuno Bay [75], freshwater sediments of Lake Ørn [28,76] and Lake Cadagno [10], freshwater wetland [77], alpine wetlands [25], and deep groundwater [53]. These environments are generally characterized by high sedimentation rates or substantial iron oxide inputs from rock weathering or anthropogenic sources, providing the necessary electron acceptors for metal-dependent AOM. The geochemical features of Budo Pond include low sulfate levels and anoxic iron-rich conditions with Fe^{2+} concentrations reaching 740 μM at a depth of just a few centimeters. These geochemical conditions are thought to serve as modern analogs of the Archaean oceans, which had vastly different ocean-atmosphere systems compared to those existing today. Before the Great Oxidation Event (GOE), the atmosphere had low oxygen levels, and seawater contained low sulfate levels, generally being anoxic and ferruginous [78–80]. Due to the GOE, iron-rich sediments were widely deposited. Fe-AOM processes may have played a crucial role in methane removal in the early Earth's oceans by linking carbon and iron cycles, preventing methane from diffusing into the overlying water or atmosphere, and significantly influencing the climatic conditions of early Earth.

Conclusions

AOM occurred at the groundwater discharge point of Budo Pond. The potential rate was determined using radiotracer-based activity measurements, which revealed the highest rate

at a depth of 2.5 cm in the upper sediment. Several geochemical features were observed in the shallow zone: (1) methane depletion with Fe^{2+} enrichment, (2) levels of other electron acceptors several orders of magnitude lower, (3) production of isotopically light DIC, and (4) a distinct peak of isotopically light TOC. Molecular biology analyses targeting the 16S rRNA and *mcrA* genes revealed the dominance of the anaerobic methanotrophs of Methanoperedenaceae. All lines of evidence suggest that methane removal is primarily coupled with iron reduction in this ferruginous freshwater system, with Methanoperedenaceae members identified as the microorganisms responsible for the observed Fe-AOM. The fresh supply of reactive iron oxides likely stimulates Fe-AOM in the surface sediments of Budo Pond, making it an ideal site for further studies on the role and regulation of AOM in natural environments with elevated iron concentrations.

Supporting information

S1 Table. Details of qPCR experiments conducted in this study.
(PDF)

S2 Table. Summary of geochemical and microbiological raw data used in this study.
(PDF)

S3 Table. Summary of the 16S rRNA gene amplicon libraries.
(PDF)

S1 Fig. Location of sampling sites. Overview of the groundwater discharge point of Budo Pond.
(PDF)

S2 Fig. Depth profiles of pore water Na, K, Cl, Mg, Ca, TOC, and the oxygen isotopic composition of water. The red-shaded layers represent the possible depth ranges of active Fe-AOM, as determined in Fig 1.
(PDF)

S3 Fig. Rarefaction curves for the 16S rRNA gene amplicon libraries of the sediment.
(PDF)

S4 Fig. Beta-diversity visualized using principal coordinate analysis (PCoA). The two principal coordinate axes explain 75.83% of variation.
(PDF)

S5 Fig. Fluorescence microscopic image of microbial cells from the Budo Pond sediment. Sediment samples at depths of 1.5 cm (A) and 4.5 cm (B) were selected as examples to show cell morphology.
(PDF)

Acknowledgments

We are grateful to the reviewers for their helpful comments and suggestions.

Author contributions

Conceptualization: Katsunori Yanagawa.

Data curation: Katsunori Yanagawa, Misaki Okabeppu, Sakiko Kikuchi, Fumito Shiraishi, Yumiko Nakajima, Akihiro Kano.

Formal analysis: Katsunori Yanagawa.

Funding acquisition: Katsunori Yanagawa.

Investigation: Katsunori Yanagawa, Fumito Shiraishi.

Methodology: Katsunori Yanagawa, Misaki Okabeppu, Sakiko Kikuchi, Yumiko Nakajima.

Project administration: Katsunori Yanagawa.

Resources: Katsunori Yanagawa, Fumito Shiraishi, Yumiko Nakajima, Akihiro Kano.

Software: Katsunori Yanagawa.

Supervision: Katsunori Yanagawa.

Validation: Katsunori Yanagawa.

Visualization: Katsunori Yanagawa.

Writing – original draft: Katsunori Yanagawa.

Writing – review & editing: Katsunori Yanagawa.

References

1. Etminan M, et al. Radiative forcing of carbon dioxide, methane, and nitrous oxide: A significant revision of the methane radiative forcing. Geophysical Research Letters. 2016;43(24):12614–23.
2. Kirschke S, Bousquet P, Ciais P, Saunois M, Pison I, Röckmann T, et al. Three decades of global methane sources and sinks. Nature Geoscience. 2013;6(10):813–23.
3. Lan X, Thoning KW, Dlugokencky EJ. Trends in globally-averaged CH4, N2O, and SF6 determined from NOAA Global Monitoring Laboratory measurements. Version 2024–06; 2022.
4. Rosentreter JA, et al. Half of global methane emissions come from highly variable aquatic ecosystem sources. Nature Geosci. 2021;14(4):225–30.
5. Knittel K, Boetius A. Anaerobic oxidation of methane: progress with an unknown process. Annu Rev Microbiol. 2009;63:311–34. https://doi.org/10.1146/annurev.micro.61.080706.093130 PMID: 19575572
6. Iversen N, Jorgensen BB. Anaerobic methane oxidation rates at the sulfate methane transition in marine-sediments from Kattegat and Skagerrak (Denmark). Limnol Oceanogr. 1985;30(5):944–55.
7. Reeburgh WS. Oceanic methane biogeochemistry. Chem. Rev. 2007.107(2):486–513. https://doi.org/10.1021/cr050362v PMID: 17261072
8. Hinrichs KU, Boetius A. The anaerobic oxidation of methane: new insights in microbial ecology and biogeochemistry, in Ocean margin systems. Wefer G, et al, editors. Berlin, Germany: Springer. 2002. p. 457–77.
9. Prasitwuttisak W, Araki S, Yanagawa K. Methanogenic archaeal community structure in estuary sediments of the Onga River, northern Kyushu Island, Japan. Laguna. 2022;29133–43.
10. Schubert CJ, Vazquez F, Lösekann-Behrens T, Knittel K, Tonolla M, Boetius A. Evidence for anaerobic oxidation of methane in sediments of a freshwater system (Lago di Cadagno). FEMS Microbiol Ecol. 2011;76(1):26–38. https://doi.org/10.1111/j.1574-6941.2010.01036.x PMID: 21244447
11. Segarra KEA, Schubotz F, Samarkin V, Yoshinaga MY, Hinrichs K-U, Joye SB. High rates of anaerobic methane oxidation in freshwater wetlands reduce potential atmospheric methane emissions. Nat Commun. 2015;6:7477. https://doi.org/10.1038/ncomms8477 PMID: 26123199
12. Haroon MF, Hu S, Shi Y, Imelfort M, Keller J, Hugenholtz P, et al. Anaerobic oxidation of methane coupled to nitrate reduction in a novel archaeal lineage. Nature. 2013;500(7464):567–70. https://doi.org/10.1038/nature12375 PMID: 23892779
13. Leu AO, Cai C, McIlroy SJ, Southam G, Orphan VJ, Yuan Z, et al. Anaerobic methane oxidation coupled to manganese reduction by members of the Methanoperedenaceae. ISME J. 2020;14(4):1030–41. https://doi.org/10.1038/s41396-020-0590-x PMID: 31988473
14. Beal EJ, House CH, Orphan VJ. Manganese- and iron-dependent marine methane oxidation. Science. 2009;325(5937):184–7. https://doi.org/10.1126/science.1169984 PMID: 19589998
15. Cai C, Leu AO, Xie G-J, Guo J, Feng Y, Zhao J-X, et al. A methanotrophic archaeon couples anaerobic oxidation of methane to Fe(III) reduction. ISME J. 2018;12(8):1929–39. https://doi.org/10.1038/s41396-018-0109-x PMID: 29662147
16. Bar-Or I, Ben-Dov E, Kushmaro A, Eckert W, Sivan O. Methane-related changes in prokaryotes along geochemical profiles in sediments of Lake Kinneret (Israel). Biogeosciences. 2015;12(10):2847–60. https://doi.org/10.5194/bg-12-2847-2015

17. Oni O, Miyatake T, Kasten S, Richter-Heitmann T, Fischer D, Wagenknecht L, et al. Distinct microbial populations are tightly linked to the profile of dissolved iron in the methanic sediments of the Helgoland mud area, North Sea. Front Microbiol. 2015;6:365. https://doi.org/10.3389/fmicb.2015.00365 PMID: 25983723

18. Shi L-D, et al. Coupled anaerobic methane oxidation and reductive arsenic mobilization in wetland soils. Nature Geoscience. 2020;13(12):799–805. https://doi.org/insert_doi_here_if_available

19. Bai Y-N, Wang X-N, Wu J, Lu Y-Z, Fu L, Zhang F, et al. Humic substances as electron acceptors for anaerobic oxidation of methane driven by ANME-2d. Water Res. 2019;164:114935. https://doi.org/10.1016/j.watres.2019.114935 PMID: 31387057

20. Valenzuela EI, Prieto-Davó A, López-Lozano NE, Hernández-Eligio A, Vega-Alvarado L, Juárez K, et al. Anaerobic methane oxidation driven by microbial reduction of natural organic matter in a tropical Wetland. Appl Environ Microbiol. 2017;83(11):e00645–17. https://doi.org/10.1128/AEM.00645-17 PMID: 28341676

21. Egger M, Rasigraf O, Sapart CJ, Jilbert T, Jetten MSM, Röckmann T, et al. Iron-mediated anaerobic oxidation of methane in brackish coastal sediments. Environ Sci Technol. 2015;49(1):277–83. https://doi.org/10.1021/es503663z PMID: 25412274

22. Rooze J, et al. Iron-dependent anaerobic oxidation of methane in coastal surface sediments: potential controls and impact. Limnol. Oceanogr. 2016. 61(S1):S267–S282.

23. Aromokeye DA, Kulkarni AC, Elvert M, Wegener G, Henkel S, Coffinet S, et al. Rates and Microbial Players of Iron-Driven Anaerobic Oxidation of Methane in Methanic Marine Sediments. Front Microbiol. 2020;10:3041. https://doi.org/10.3389/fmicb.2019.03041 PMID: 32010098

24. Ettwig KF, Zhu B, Speth D, Keltjens JT, Jetten MSM, Kartal B. Archaea catalyze iron-dependent anaerobic oxidation of methane. Proc Natl Acad Sci U S A. 2016;113(45):12792–6. https://doi.org/10.1073/pnas.1609534113 PMID: 27791118

25. Chen L, Li L, Zhang S, Zhang W, Xue K, Wang Y, et al. Anaerobic methane oxidation linked to Fe(III) reduction in a Candidatus Methanoperedens-enriched consortium from the cold Zoige wetland at Tibetan Plateau. Environ Microbiol. 2022;24(2):614–25. https://doi.org/10.1111/1462-2920.15848 PMID: 34951085

26. Ino K, Hernsdorf AW, Konno U, Kouduka M, Yanagawa K, Kato S, et al. Ecological and genomic profiling of anaerobic methane-oxidizing archaea in a deep granitic environment. ISME J. 2018;12(1):31–47. https://doi.org/10.1038/ismej.2017.140 PMID: 28885627

27. Yanagawa K, Kouduka M, Nakamura Y, Hachikubo A, Tomaru H, Suzuki Y. Distinct microbial communities thriving in gas hydrate-associated sediments from the eastern Japan Sea. Journal of Asian Earth Sciences. 2014;90:243–9. https://doi.org/10.1016/j.jseaes.2013.10.019

28. Weber HS, Habicht KS, Thamdrup B. Anaerobic Methanotrophic Archaea of the ANME-2d Cluster Are Active in a Low-sulfate, Iron-rich Freshwater Sediment. Front Microbiol. 2017;8:619. https://doi.org/10.3389/fmicb.2017.00619 PMID: 28446901

29. Lu Y-Z, Fu L, Ding J, Ding Z-W, Li N, Zeng RJ. Cr(VI) reduction coupled with anaerobic oxidation of methane in a laboratory reactor. Water Res. 2016;102:445–52. https://doi.org/10.1016/j.watres.2016.06.065 PMID: 27395029

30. Yang H, Yu S, Lu H. Iron-coupled anaerobic oxidation of methane in marine sediments: a review. J Mar Sci Eng. 2021;9(8):875.

31. Kikuchi S, et al. Limited reduction of ferrihydrite encrusted by goethite in freshwater sediment. Geobiology, 2016;14(4):374–89.

32. Kato S, Kikuchi S, Kashiwabara T, Takahashi Y, Suzuki K, Itoh T, et al. Prokaryotic Abundance and Community Composition in a Freshwater Iron-Rich Microbial Mat at Circumneutral pH. Geomicrobiology J. 2012;29(10):896–905. https://doi.org/10.1080/01490451.2011.635763

33. Takahashi Y, Hirata T, Shimizu H, Ozaki T, Fortin D. A rare earth element signature of bacteria in natural waters? Chemical Geology. 2007;244(3–4):569–83. https://doi.org/10.1016/j.chemgeo.2007.07.005

34. Stookey LL. Ferrozine - a new spectrophotometric reagent for iron. Anal Chem. 1970;42(7):779–81.

35. Cline JD. Spectrophotometric determination of hydrogen sulfide in natural waters. Limnol Oceanogr. 1969;14(3):454–8.

36. Hachikubo A, et al. Molecular and isotopic composition of volatiles in gas hydrates and in sediment from the Joetsu Basin, eastern margin of the Japan Sea. Energies. 2015;8(6):4647–66. https://doi.org/10.3390/en8064647

37. Kano A, et al. Gas hydrate estimates in muddy sediments from the oxygen isotope of water fraction. Chemical Geology. 2017;470:107–15.

38. Tasumi E, et al. In vitro high-pressure incubation and activity measurement of deep-sea methanogenic archaea, in Hydrocarbon and Lipid Microbiology Protocols. McGenity TJ, Timmis KN, Nogales B, editors. Springer; 2015. p. 1–14.

39. Yanagawa K, Ijiri A, Breuker A, Sakai S, Miyoshi Y, Kawagucci S, et al. Defining boundaries for the distribution of microbial communities beneath the sediment-buried, hydrothermally active seafloor. ISME J. 2017;11(2):529–42. https://doi.org/10.1038/ismej.2016.119 PMID: 27754478

40. Alperin MJ, Reeburgh WS, Whiticar MJ. Carbon and hydrogen isotope fractionation resulting from anaerobic methane oxidation. Global Biogeochemical Cycles. 1988;2(3):279–88. https://doi.org/10.1029/gb002i003p00279

41. Prasitwuttisak W, Hoshiko Y, Maeda T, Haraguchi A, Yanagawa K. Microbial Community Structures and Methanogenic Functions in Wetland Peat Soils. Microbes Environ. 2022;37(3):ME22004. https://doi.org/10.1264/jsme2.ME22004 PMID: 35851269

42. Caporaso JG, Lauber CL, Walters WA, Berg-Lyons D, Lozupone CA, Turnbaugh PJ, et al. Global patterns of 16S rRNA diversity at a depth of millions of sequences per sample. Proc Natl Acad Sci U S A. 2011;108(Suppl 1):4516–22. https://doi.org/10.1073/pnas.1000080107 PMID: 20534432

43. Bolyen E, Rideout JR, Dillon MR, Bokulich NA, Abnet CC, Al-Ghalith GA, et al. Reproducible, interactive, scalable and extensible microbiome data science using QIIME 2. Nat Biotechnol. 2019;37(8):852–7. https://doi.org/10.1038/s41587-019-0209-9 PMID: 31341288

44. Callahan BJ, McMurdie PJ, Rosen MJ, Han AW, Johnson AJA, Holmes SP. DADA2: High-resolution sample inference from Illumina amplicon data. Nat Methods. 2016;13(7):581–3. https://doi.org/10.1038/nmeth.3869 PMID: 27214047

45. Katoh K, Misawa K, Kuma K, Miyata T. MAFFT: a novel method for rapid multiple sequence alignment based on fast Fourier transform. Nucleic Acids Res. 2002;30(14):3059–66. https://doi.org/10.1093/nar/gkf436 PMID: 12136088

46. Price MN, Dehal PS, Arkin AP. FastTree 2--approximately maximum-likelihood trees for large alignments. PLoS One. 2010;5(3):e9490. https://doi.org/10.1371/journal.pone.0009490

47. Asamatsu K, Yoshitake K, Saito M, Prasitwuttisak W, Ishibashi J-I, Tsutsumi A, et al. A Novel Archaeal Lineage in Boiling Hot Springs around Oyasukyo Gorge (Akita, Japan). Microbes Environ. 2021;36(4):ME21048. https://doi.org/10.1264/jsme2.ME21048 PMID: 34819404

48. Takai K, Horikoshi K. Rapid detection and quantification of members of the archaeal community by quantitative PCR using fluorogenic probes. Applied and Environmental Microbiology. 2000;66(11):5066–72.

49. Nunoura T, Oida H, Miyazaki J, Miyashita A, Imachi H, Takai K. Quantification of mcrA by fluorescent PCR in methanogenic and methanotrophic microbial communities. FEMS Microbiol Ecol. 2008;64(2):240–7. https://doi.org/10.1111/j.1574-6941.2008.00451.x PMID: 18318714

50. Ludwig W, Strunk O, Westram R, Richter L, Meier H, , et al. ARB: a software environment for sequence data. Nucleic Acids Res. 2004;32(4):1363–71. https://doi.org/10.1093/nar/gkh293 PMID: 14985472

51. Peckmann J, Thiel V. Carbon cycling at ancient methane–seeps. Chemical Geology. 2004;205(3):443–67.

52. Yanagawa K, Shiraishi F, Tanigawa Y, Maeda T, Mustapha NA, Owari S, et al. Endolithic Microbial Habitats Hosted in Carbonate Nodules Currently Forming within Sediment at a High Methane Flux Site in the Sea of Japan. Geosciences. 2019;9(11):463. https://doi.org/10.3390/geosciences9110463

53. Nishimura H, Kouduka M, Fukuda A, Ishimura T, Amano Y, Beppu H, et al. Anaerobic methane-oxidizing activity in a deep underground borehole dominantly colonized by Ca. Methanoperedenaceae. Environ Microbiol Rep. 2023;15(3):197–205. https://doi.org/10.1111/1758-2229.13146 PMID: 36779262

54. Emerson D, Moyer C. Isolation and characterization of novel iron-oxidizing bacteria that grow at circumneutral pH. Appl Environ Microbiol. 1997;63(12):4784–92. https://doi.org/10.1128/aem.63.12.4784-4792.1997 PMID: 9406396

55. Jørgensen BB, Nelson DC. Sulfide oxidation in marine sediments: Geochemistry meets microbiology, in Sulfur Biogeochemistry - Past and Present. Amend JP, Edwards KJ, Lyons TW, editors. Geological Society of America; 2004.

56. McInerney MJ, Sieber JR, Gunsalus RP. Syntrophy in anaerobic global carbon cycles. Curr Opin Biotechnol. 2009;20(6):623–32. https://doi.org/10.1016/j.copbio.2009.10.001 PMID: 19897353

57. Begmatov S, Beletsky AV, Dedysh SN, Mardanov AV, Ravin NV. Genome analysis of the candidate phylum MBNT15 bacterium from a boreal peatland predicted its respiratory versatility

and dissimilatory iron metabolism. Front Microbiol. 2022;13:951761. https://doi.org/10.3389/fmicb.2022.951761 PMID: 35992725

58. Kolinko S, Richter M, Glöckner F-O, Brachmann A, Schüler D. Single-cell genomics of uncultivated deep-branching magnetotactic bacteria reveals a conserved set of magnetosome genes. Environ Microbiol. 2016;18(1):21–37. https://doi.org/10.1111/1462-2920.12907 PMID: 26060021

59. Castelle CJ, Hug LA, Wrighton KC, Thomas BC, Williams KH, Wu D, et al. Extraordinary phylogenetic diversity and metabolic versatility in aquifer sediment. Nat Commun. 2013;4:2120. https://doi.org/10.1038/ncomms3120 PMID: 23979677

60. Baker BJ, Lazar CS, Teske AP, Dick GJ. Genomic resolution of linkages in carbon, nitrogen, and sulfur cycling among widespread estuary sediment bacteria. Microbiome. 2015;3:14. https://doi.org/10.1186/s40168-015-0077-6 PMID: 25922666

61. Mori K, Sunamura M, Yanagawa K, Ishibashi J, Miyoshi Y, Iino T, et al. First cultivation and ecological investigation of a bacterium affiliated with the candidate phylum OP5 from hot springs. Appl Environ Microbiol. 2008;74(20):6223–9. https://doi.org/10.1128/AEM.01351-08 PMID: 18776034

62. Dyksma S, Gallert C. Effect of magnetite addition on transcriptional profiles of syntrophic Bacteria and Archaea during anaerobic digestion of propionate in wastewater sludge. Environ Microbiol Rep. 2022;14(4):664–78. https://doi.org/10.1111/1758-2229.13080 PMID: 35615789

63. Tan S, Liu J, Fang Y, Hedlund BP, Lian Z-H, Huang L-Y, et al. Insights into ecological role of a new deltaproteobacterial order Candidatus Acidulodesulfobacterales by metagenomics and metatranscriptomics. ISME J. 2019;13(8):2044–57. https://doi.org/10.1038/s41396-019-0415-y PMID: 30962514

64. Weber KA, Achenbach LA, Coates JD. Microorganisms pumping iron: anaerobic microbial iron oxidation and reduction. Nat Rev Microbiol. 2006;4(10):752–64. https://doi.org/10.1038/nrmicro1490 PMID: 16980937

65. Fu L, Li S-W, Ding Z-W, Ding J, Lu Y-Z, Zeng RJ. Iron reduction in the DAMO/Shewanella oneidensis MR-1 coculture system and the fate of Fe(II). Water Res. 2016;88:808–15. https://doi.org/10.1016/j.watres.2015.11.011 PMID: 26599434

66. Suzuki T, Hashimoto H, Itadani A, Matsumoto N, Kunoh H, Takada J. Silicon and phosphorus linkage with iron via oxygen in the amorphous matrix of Gallionella ferruginea stalks. Appl Environ Microbiol. 2012;78(1):236–41. https://doi.org/10.1128/AEM.05913-11 PMID: 22020519

67. Lovley DR, Phillips EJ. Availability of ferric iron for microbial reduction in bottom sediments of the freshwater tidal potomac river. Appl Environ Microbiol. 1986;52(4):751–7. https://doi.org/10.1128/aem.52.4.751-757.1986 PMID: 16347168

68. Liu C, Kota S, Zachara JM, Fredrickson JK, Brinkman CK. Kinetic analysis of the bacterial reduction of goethite. Environ Sci Technol. 2001;35(12):2482–90. https://doi.org/10.1021/es001956c PMID: 11432552

69. Fredrickson JK, Zachara JM, Kennedy DW, Dong H, Onstott TC, Hinman NW, et al. Biogenic iron mineralization accompanying the dissimilatory reduction of hydrous ferric oxide by a groundwater bacterium. Geochimica et Cosmochimica Acta. 1998;62(19–20):3239–57. https://doi.org/10.1016/s0016-7037(98)00243-9

70. Pallud C, Kausch M, Fendorf S, Meile C. Spatial patterns and modeling of reductive ferrihydrite transformation observed in artificial soil aggregates. Environ Sci Technol. 2010;44(1):74–9. https://doi.org/10.1021/es901736t PMID: 20039736

71. Sivan O, Adler M, Pearson A, Gelman F, Bar-Or I, John SG, et al. Geochemical evidence for iron-mediated anaerobic oxidation of methane. Limnology & Oceanography. 2011;56(4):1536–44. https://doi.org/10.4319/lo.2011.56.4.1536

72. Norði Kà., Thamdrup B, Schubert CJ. Anaerobic oxidation of methane in an iron-rich Danish freshwater lake sediment. Limnology and Oceanography. 2013;58(2):546–54.

73. Crowe SA, Katsev S, Leslie K, Sturm A, Magen C, Nomosatryo S, et al. The methane cycle in ferruginous Lake Matano. Geobiology. 2011;9(1):61–78. https://doi.org/10.1111/j.1472-4669.2010.00257.x PMID: 20854329

74. Riedinger N, Formolo MJ, Lyons TW, Henkel S, Beck A, Kasten S. An inorganic geochemical argument for coupled anaerobic oxidation of methane and iron reduction in marine sediments. Geobiology. 2014;12(2):172–81. https://doi.org/10.1111/gbi.12077 PMID: 24460948

75. Roland FAE, Borges AV, Darchambeau F, Llirós M, Descy J-P, Morana C. The possible occurrence of iron-dependent anaerobic methane oxidation in an Archean Ocean analogue. Sci Rep. 2021;11(1):1597. https://doi.org/10.1038/s41598-021-81210-x PMID: 33452366

76. Mostovaya A. Sulfate-and iron-dependent anaerobic methane oxidation occurring side-by-side in freshwater lake sediment. Limnology and Oceanography. 2022;67(1):231–46.

77. Shen LD, et al. Detection and quantification of Candidatus Methanoperedens-like archaea in freshwater wetland soils. Microbial Ecology. 2023;85(2):441–53.

78. Crowe SA, Paris G, Katsev S, Jones C, Kim S-T, Zerkle AL, et al. Sulfate was a trace constituent of Archean seawater. Science. 2014;346(6210):735–9. https://doi.org/10.1126/science.1258966 PMID: 25378621

79. Konhauser KO, Newman DK, Kappler A. The potential significance of microbial Fe(III) reduction during deposition of Precambrian banded iron formations. Geobiology. 2005;3(3):167–77.

80. Planavsky NJ, McGoldrick P, Scott CT, Li C, Reinhard CT, Kelly AE, et al. Widespread iron-rich conditions in the mid-Proterozoic ocean. Nature. 2011;477(7365):448–51. https://doi.org/10.1038/nature10327 PMID: 21900895